Hydrothermal Synthesis of Cobalt- Doped Hydroxyapatite Nanoparticles: Structure, Magnetic Behaviour, Bioactivity and Antibacterial Activity

N. Yazdani, J. Javadpour, B. Eftekhari Yekta and M. Hamrang

** javadpourj@iust.ac.ir*

Received: January 2018 **Revised: August 2018** **Accepted: October 2018**

School of Metallurgy and Materials Engineering, Iran University of Science and Technology, Tehran, Iran.

DOI: 10.22068/ijmse.16.1.39

Abstract: *This study focuses on the physical, magnetic, biological and antibacterial behavior of cobalt-doped hydroxyapatite (HAp) powder samples. Pure and cobalt- doped HAp nanoparticles were synthesized by hydrothermal method. Calcium nitrate, di- ammonium hydrogen phosphate and cobalt nitrate were used as precursor materials. The synthesized powders were characterized using x-ray diffraction pattern (XRD), fourier transform infrared spectroscopy (FTIR), field emission scanning electron microscopy (FESEM), vibrating sample magnetometer (VSM), raman spectroscopy as well as MTT assay and cell adhesion test. Disc diffusion method was used to investigate antibacterial activity of the samples. The results confirmed the substitution of Ca by Co ions in the HAp lattice. In addition, this substitution induced size reduction and morphology change in HAp particles. All cobalt substituted HAp powder samples displayed paramagnetic properties, as opposed to the diamagnetic behavior observed in the pure HAp samples. In addition, these nanoparticles exhibited cell adhesion, cell viability and antibacterial activity against S.aureus bacteria.*

Keywords: *Hydroxyapatite, Cobalt- doped hydroxyapatite, Hydrothermal, Paramagnetic, Antibacterial activity*

1. INTRODUCTION

Although natural bone tissues possess excellent intrinsic self- repairing capability, its self- renewal process is generally delayed in critical- sized bone defects [1-3]. There are variety of mechanical, electrical and magnetic external stimulus which can facilitate bone regeneration process [4]. For example, static magnetic field (SMF) has shown to be an effective approach in accelerating bone fracture healing as a result of interaction between the magnetic field and biological processes in the bone [4,5]. As a result, there has been an increase in the use of magnetic nanoparticles (MNps) in biomedical applications for bone regeneration [6-7]. One of the most common type of magnetic nanoparticles used in biomedical field is iron oxide (Fe_2O_3) particles. However, there has been an interest in other magnetic particles due to the toxicity observed with the use of Fe_2O_3 particles [8].

HAp particles with the chemical formula of $Ca_{10}(PO_4)_6(OH)_2$ are widely applied to fill bone defects in view of their great biocompatibility, bioactivity and osteoconductivity [9]. However, bacterial adsorption on the HAp surface may result in implant infection and the loss of the bone support [10,11]. With the aim of providing an effective protection against this type of infection, some metal ions such as Ag^+, Sr^{2+} and Cu^{2+} with antibacterial activity have been incorporated in the HAp lattice structure [12-13]. The possibility to replace Ca^{2+} ions in the HAp lattice with other ions is an important characteristics of HAp lattice [14]. Ionic substitution has shown to have a significant effect on the biological properties of HAp. As an illustration, incorporation of Ag in the HAp lattice demonstrated considerable antibacterial activity compared to the undoped HAp counterparts [15].

Cobalt (Co), iron (Fe) and nickel (Ni) are the magnetic ions exploited to induce magnetic property in the HAp nanoparticles [16-23]. Co is used as one of the alloy components in the orthopedic implants and prostheses due to its high strength and wear resistance [24]. In addition, cobalt is also the active center of cobalamin known as vitamin B-12 which plays a prevailing role in DNA production [25]. Very limited studies have been done on cobalt- doped HAp. In an earlier report, both Kramer and Chandra have stated that cobalt- doped HAp display paramagnetic properties as opposed to diamagnetic behavior observed in the pure HAp [19-26]. In another study, it was reported

[DOI: 10.22068/ijmse.16.1.39]

that increasing cobalt content up to 12 wt.% was beneficial on osteogenesis and new bone formation [27]. Additionally, the improvement of osteogenic and angiogenic properties of HAp was observed in cobalt- magnesium-doped HAp [28]. Due to the lack of extensive literature on the synthesis and characterization of cobalt- doped HAp, the effect of Co content (1-5 wt. % Co) on the crystal structure, morphology, cell viability, antibacterial and magnetic properties of HAp are investigated in the current study.

2. MATERIALS AND METHODS

2.1. Synthesis of HAp and Cobalt- Doped HAp Nanoparticles

Powders of HAp and cobalt- doped HAp (1-5wt. %) referred to as HAp, CoHAp1, CoHAp2, CoHAp3, CoHAp4 and CoHAp5 respectively were synthesized via hydrothermal process. Calcium nitrate tetrahydrate ($Ca(NO_3)_2.\ 4H_2O$, Merck), diammonium hydrogen phosphate. ($(NH_4)_2HPO_4$, Merck) and cobalt (II) nitrate hexahydrate ($Co(NO_3)_2.\ 6H_2O$, Merck) were used as starting materials. The (Ca + Co)/ P molar ratio was kept at 1.67. Details on the sample compositions and their coding is provided in Table 1.

For the synthesis of HAp, initially all reagents were dissolved in 30 ml distilled water. Diammonium hydrogen phosphate was added drop wise to calcium nitrate solution, over a period of 20 minutes, at room temperature. Ammonia was added to the solution to adjust the pH value at 10. After 20 minutes of mixing, the resulted suspension was transferred to well-sealed polytetrafluoroethylene (PTFE) cell in a stainless steel container and was hydrothermally heated at 200°C for 8h. The resulting precipitate was separated by centrifuge and washed with distilled water three times and finally dried at 80°C for 24h.

For the synthesis of cobalt- doped HAp, proper amount of cobalt nitrate solution, for 1, 2, 3, 4 and 5wt. % substitutions, was mixed with calcium nitrate solution. Cobalt- doped HAp nanoparticles displayed violet colour, as opposed to the white colour of pure HAp. The change in colour was intensified with the increase in the cobalt content.

2. 2. Sample Characterization

2. 2. 1. X-Ray Diffraction (XRD)

The crystal structure of the samples was determined by X-ray powder diffraction (XRD, JEOL JDX8030), using CuKα radiation. The patterns were scanned in the 2θ range of 20- 80°. The peak shift in the cobalt- doped HAp was calculated by using the position of the peaks in the 2θ range of 25- 45° [29]. The phase compositions of the samples were identified by analyzing the XRD patterns using X'Pert High Score software. The quantitative evaluation of cell parameters was performed using Bragg's law.

Table 1. Sample codes and compositions

Sample code	Chemical formula $Ca_{10-X}\ Cox\ (PO_4)_6(OH)_2$	X	Cobalt weight percentage (%.wt)
HAp	$Ca_{10}\ (PO_4)_6(OH)_2$	0	0
Co HAp 1	$Ca_{9.829}\ Co_{0.171}\ (PO_4)_6(OH)_2$	0.171	1
Co HAp 2	$Ca_{9.658}\ Co_{0.342}\ (PO_4)_6(OH)_2$	0.342	2
Co HAp 3	$Ca_{9.487}\ Co_{0.513}\ (PO_4)_6(OH)_2$	0.513	3
Co HAp 4	$Ca_{9.316}Co_{0.684}\ (PO_4)_6(OH)_2$	0.684	4
Co HAp 5	$Ca_{9.145}\ Co_{0.855}(PO_4)_6(OH)_2$	0.855	5

[DOI: 10.22068/ijmse.16.1.39]

2. 2. 2. Fourier Transform Infra red Spectroscopy (FTIR)

FTIR investigation of HAp and cobalt- doped HAp samples was carried out on a Shimadzu FTIR-8400S spectrometer in the wavenumber range of 400- 4000 cm-1 using the KBr disc technique.

2. 2. 3. Field emission Scanning Electron Microscope (FESEM)

Information about morphology of the powder samples was obtained using field emission scanning electron microscope (FESEM, TESCAN MIRA) operating at 15kV. The powders for FESEM examination were dispersed in ethanol ultrasonically and coated by a thin layer of gold.

2. 2. 4. Vibrating Sample Magnetometer (VSM)

Magnetic property of powder samples were investigated by conducting vibrating sample magnetometer (VSM, MDk6) at room temperature. Magnetization vs. magnetic field (M vs, H) curves were recorded in a magnetic field cycle of -15 to 15 kOe.

2. 2. 5. Raman Spectroscopy

The possible effect of cobalt- substitution on the structure was also followed by conducting Raman spectroscopy (SENTERRA) at room temperature. The spectra was collected in the range of 200- 3500 cm^{-1} using 785 nm laser excitation with 3 cm^{-1} spectral resolution.

2. 2. 6. MTT Assay

MTT assay (3-(4,5- dimethylthiazol-2-yl)-2,5-diphenyl tetrazolium bromide) was employed to assess the in vitro cytotoxicity in the cobalt- doped HAp powders. This is a tetrazolium reduction test assessing cell viability with conversion of MTT into formazan crystals. The test conducted by powder extraction procedure according to ISO 10993- 5 standard [30]. 0.1 g of powder samples with 0, 1, 2, 3, 4 and 5 wt. % cobalt were added into 1 ml of culture medium and were incubated for 7 days at 37°C in a 5% CO_2 atmosphere. Afterwards, $1x10^4$ MG63 cells/ well were placed into a 96- well plate. It is worth noting that MG63 is considered as human osteoblast-like cells. After 24 h incubation at 37°C, the culture medium in each well was exchanged by 90 µl powder extracts and 10 µl FBS. After 24 h, the medium in each well was eliminated and replaced by 100 µl MTT (Sigma, USA) at a density of 0.5 mg/ ml and incubated at 37°C for 4 h. Subsequently, the purple formazan crystals were dissolved in 100 µl isopropanol (Sigma, USA) added per well. After 15 min incubation of plates at 37°C, the optical density (OD) of formazan in isopropanol was recorded at 545 nm using multiwell plate reader (STAT FAX 2100, USA). The resulting absorbance values were normalized with respect to the control sample.

2. 2. 7. Cell Adhesion

To evaluate cell attachment, MG63 cells were seeded onto disk- shaped samples (1×10^4 cells/ well) pressed uniaxially (0.12 g of powder was pressed into 10 mm disk die at a pressure of 340 MPa) and incubated at 37°C in a 5wt.% CO_2 atmosphere. After 3h, the samples were washed with PBS to remove unattached cells. The cells were then fixed in 1 ml glutaraldehyde for 30 min at room temperature. Subsequently, they were washed twice with distilled water and then dried. A thin layer of gold, as a conductive material, was applied onto the samples prior to observing under scanning electron microscope.

2. 2. 8. Alkaline Phosphatase (ALP) Activity

ALP is a hydrolase enzyme which is produced during bone formation by osteoblast cells and it is considered as an indicator for osteoblast activity. In this test, MG63 cells were cultured for 5-7 days with trypsin to reach appropriate confluency. Afterwards, around 3000 cells per 50 µl culture medium including 10% fetal bovine serum (FBS) were poured on weighted powder in each well of 24 well plate and in an empty well used as control. The samples were incubated for 5-6hrs prior to cell attachment study. Subsequently 700 µl culture medium with 10% FBS was added to each well and incubated. After 7 days, 300 µl culture medium with 10%

[DOI: 10.22068/ijmse.16.1.39]

FBS was added to each well. Following this procedure, 20 µl of cell culture supernatant was obtained and para-Nitrophenylphosphate and Diethanolamine were used to estimate alkaline phosphatase release.

2. 2. 9. Antibacterial Test (Disk Diffusion Method)

The in vitro antibacterial activity of samples was carried out against three bacterial strains E.coli (Gram negative), S.aureus (Gram positive) and p. aueroginosa (Gram positive) by agar disk diffusion method in nutritive agar. The strains were inoculated in nutritive agar and incubated at 37°C for 24 h. The agar disk diffusion test was performed in culture medium (Muller-Hinton agar medium). It was heated to liquefy in water bath and then liquid agar was poured into petri dishes (diameter: 100mm) to form 4mm thick layer. 0.12 g powder (with different concentration of Co^{2+} ions concentration) was pressed into a 10 mm disk at 340 MPa pressure and autoclaved prior to test. The disks were equally distributed on the agar surface and incubated for 24 h at 37°C in the dark. After incubation, the result of antibacterial activity was performed by measuring the width of the inhibition zones (mm) around the disks.

3. RESULTS AND DISCUSSION

3. 1. Crystal Phase Analysis

Fig. 1 shows the XRD patterns of the powder samples (HAp, CoHAp1, CoHAp2, CoHAp3, CoHAp4 and CoHAp5). The formation of single phase pure and cobalt- doped HAp was confirmed by this XRD results. According to JCPDS card number 9-432, all the peaks in the XRD profiles (pure and cobalt- doped HAp) correspond very well with the standard reference pattern for hexagonal HAp structure. However, as it can be seen in these patterns, the incorporation of Co ions in the HAp structure resulted in the broader and less intense XRD peaks which may be the result of the structural strain created as a result of the difference between calcium ionic radius (0.0990 nm) and cobalt ionic radius (0.0745 nm). Using Bragg's law, a decrease in the cell parameters was observed with the presence of Co in the HAp lattice (a=b=9.4461 A°, c=6.9 A° for pure HAp and a=b=9.4146 A°, c=6.87 A° for cobalt- doped HAp sample). As a result of this decrease in the unit- cell parameters, diffraction peaks showed a shift to larger angles by around 0.1° for the CoHAp5 (Fig. 5B). A similar effect on the cell parameters was also reported by Veselinovic et al.

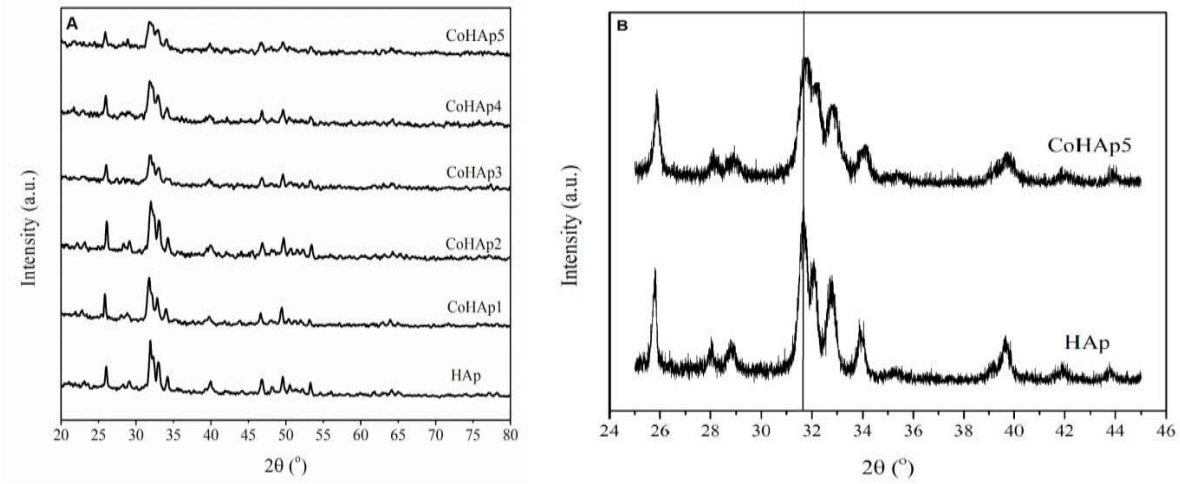

Fig. 1. (A) X-ray diffraction pattern of synthesized HAp, CoHAp1, CoHAp2, CoHAp3, CoHAp4 and CoHAp5
(B) X-ray diffraction pattern of HAp and CoHAp 5 in the 2tetha range of 24-46 with step size of 0.005

[DOI: 10.22068/ijmse.16.1.39]

[11]. Moreover, using the relation for the crystal volume ($V = \frac{\sqrt{3}}{2} a^2.c$), a decrease in cell volume from 533.1934 A° for pure HAp to 527.6376 A° for CoHAp5 was observed as a result of the smaller cobalt ion radius.

3. 2. Fourier Transform Infra-Red (FTIR) Analysis

The FTIR spectra for the synthesized HAp and CoHAp5 samples are shown in Fig. 2. The bands at 601 and 565 cm^{-1} are related to bending modes of PO_4^{3-} [19][14]. The bands related to stretching modes of PO_4^{3-} can be observed in the range of 1000-1100 cm^{-1} [31][28]. The bands at 3570 and 634 cm^{-1} are related to O-H stretching modes of HAp [19]. The weak bands between 3200 and 3500 cm^{-1} are attributed to physical adsorption of H_2O [17]. There was no obvious difference between the two spectra except the appearance of new bands in the range of 1400 - 1460 cm^{-1} in the cobalt- doped sample. These bands correspond to vibrational modes of CO_3^{2-} groups [17]. The high intensity indicates higher adsorption of CO_2 molecules by the doped sample as a result of smaller particle size and higher specific surface area.

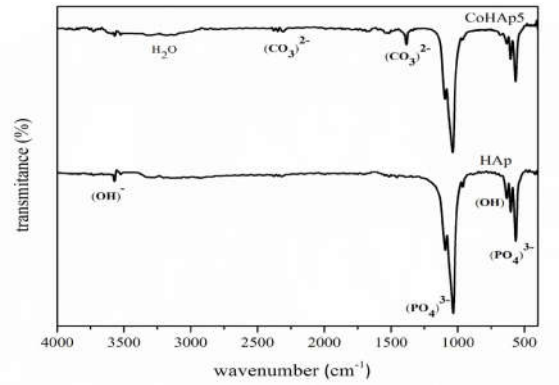

Fig. 2. FTIR spectrum of HAp and CoHAp5

3. 3. Field Emission Scanning Electron Microscope (FESEM) Analysis

FESEM micrographs of HAp, CoHAp1, CoHAp2, CoHAp3, CoHAp4 and CoHAp5 powder samples are presented in Fig. 3. As indicated in these figures, there is a change in morphology from rod-like to spherical shape with the increase in the cobalt concentration. The change in morphology has been attributed to the change in growth facet to minimize surface energy [17]. A decrease in particle size was also observed with the doping of cobalt into HAp structure. Moreover, both pure HAp and Cobalt- doped HAp samples show high degree of agglomeration.

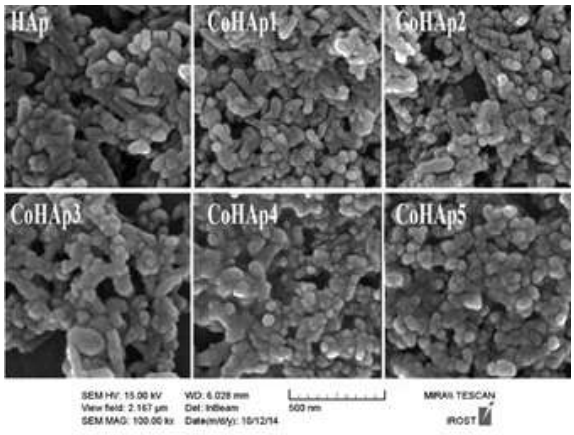

Fig. 3. FESEM images of HAp, CoHAp1, CoHAp2, CoHAp3, CoHAp4 and CoHAp5

3. 4. The Vibrating Sample Magnetometer (VSM)

The magnetization- magnetic field curve of cobalt- doped HAp samples are shown in Fig. 4. The magnetization curve for the pure HAp nanoparticles shows diamagnetic behavior. In contrast, the magnetic behavior changed from diamagnetic to paramagnetic with the presence of cobalt ions in the HAp lattice. The paramagnetic behavior in the doped samples is the direct result of Co substitution as there was no sign for the formation of magnetic phase as determined by raman spectroscopy (see Fig. 5). It is also worth noting that, there is an increase in the value of saturation magnetization with the increase in the Co content. This behavior is in agreement with the previous reports [19-22].

3. 5. Raman Spectroscopy

The possibility for the formation of magnetic phases such as cobalt oxide was also investigated by Raman spectroscopy. Fig. 5 illustrates the results of this test on HAp, CoHAp1, CoHAp2, CoHAp3, CoHAp4 and CoHAp5 samples. The band with highest intensity at 966 cm^{-1} is related to the symmetric stretching mode of P-O group,

[DOI: 10.22068/ijmse.16.1.39]

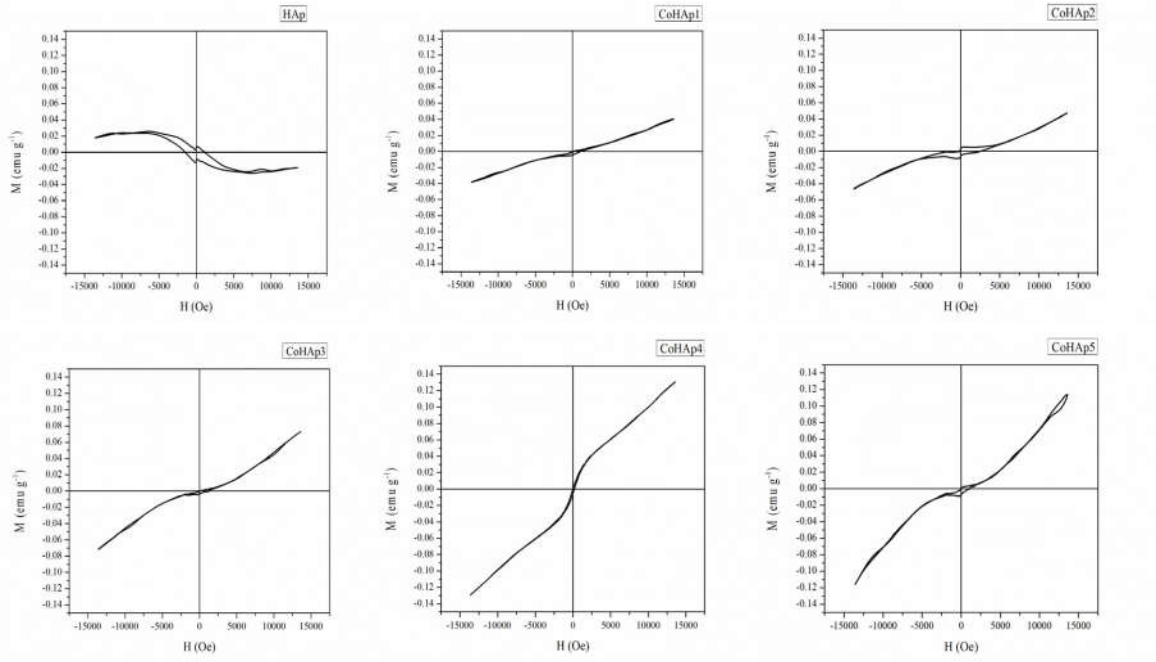

Fig. 4. Magnetic behaviour of HAp, CoHAp1, CoHAp2, CoHAp3, CoHAp4 and CoHAp5 using VSM analysis

ν_1 [31]. The bands at 1052 and 1080 cm^{-1} correspond to asymmetric stretching mode of P-O group, ν_3 [31]. The bands at 612, 595, 450 and also at 435 cm^{-1} originate from O-P-O bending mode, ν_4 and ν_2 [31]. As indicated in this Fig. there is no significant difference between the pure HAp and doped HAp samples except for their relative intensity. In addition, there are no bands indicating the presence of CoO and/or Co_3O_4 in the spectra [30].

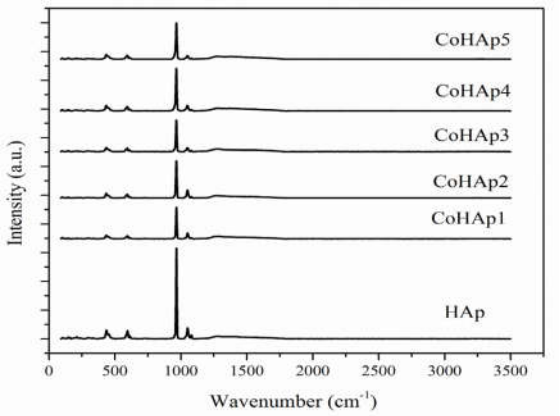

Fig. 5. Raman spectrum of HAp, CoHAp1, CoHAp2, CoHAp3, CoHAp4 and CoHAp5 samples.

3. 6. MTT Assay

Fig. 6 demonstrates the results of MTT assay for HAp, CoHAp1, CoHAp2, CoHAp3, CoHAp4 and CoHAp5 powder samples. As it is shown in this Fig., the cell viability percentage of all samples are more than 80%, except for CoHAp5 sample which is around 80%. This result confirms the acceptable mitochondrial activity of cells in the presence of Co ions in the HAp lattice. Close to 80% cell viability in the highest Co- containing sample (5 wt. % in this study) suggests that there is a critical Co loading content beyond which there is a potential for toxicity.

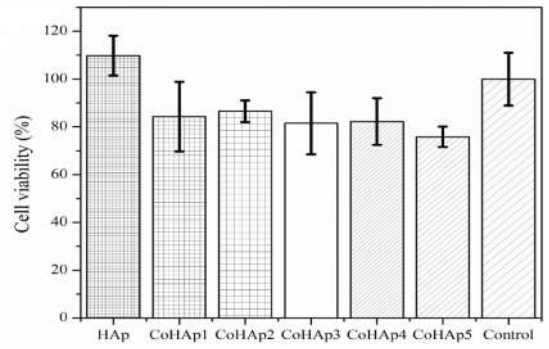

Fig. 6. MTT assay results of control, HAp, CoHAp1, CoHAp2, CoHAp3, CoHAp4 and CoHAp5

[DOI: 10.22068/ijmse.16.1.39]

3. 7. Alkaline Phosphatase Assay

Fig. 7 displays the alkaline phosphatase release levels for pure and Cobalt- doped samples after the period of 1-week direct contact with MG-63 cells. As indicated in this Fig., there is a higher ALP release for all powder extracts compared to the control sample. Of course, the highest ALP activity was observed in the presence of pure HAp powder extract. The results also points out to the fact that the cobalt content used in this study did not have an adverse on the osteoblast cell activity [32, 33].

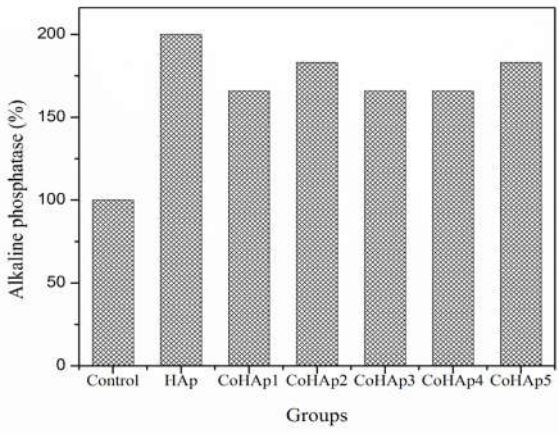

Fig. 7. Alkaline phosphatase assay results of control, HAp, CoHAp1, CoHAp2, CoHAp3, CoHAp4 and CoHAp5

3. 8. Cell Adhesion

The results for the MG-63 cell adhesion onto pure and Cobalt-doped samples are displayed in Fig. 8. As it is revealed, cell attachment has occurred on all samples and there is no obvious difference between the extent of cell attachment and their spreading on different specimens. A good cell-surface interaction is a key parameter in the subsequent cell proliferation and differentiation process [34, 35].

3. 9. Antibacterial Activity

To examine the antibacterial activity of the synthesized samples, disc diffusion method was carried out. Fig. 9 shows that with the increase in the cobalt substitution in the HAp structure, the size of area formed around the disks (zone of inhibition) is

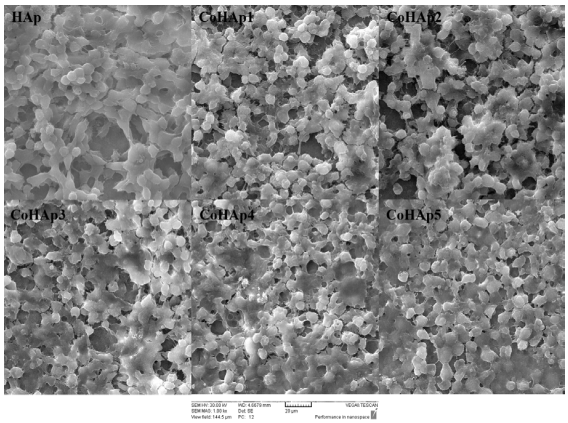

Fig. 8. SEM images of MG63 cell adhesion to HAp, CoHAp1, CoHAp2, CoHAp3, CoHAp4 and CoHAp5 substrates

increased indicating less growth for the S. aureus bactria. In contrast, as it is shown in this Fig., the E.Coli and P.aeruginosa bacteria grew considerably around the disks. This result is due to the fact that S.aureus is more sensitive than E.coli and P.aeruginosa against chemical stresses such as antibiotic due to the difference in their cell wall composition. As a result, when S.aureus bacteria encounter nanoparticles, their cell membrane reacts with nanoparticles and become punctured and destroyed [36, 37].

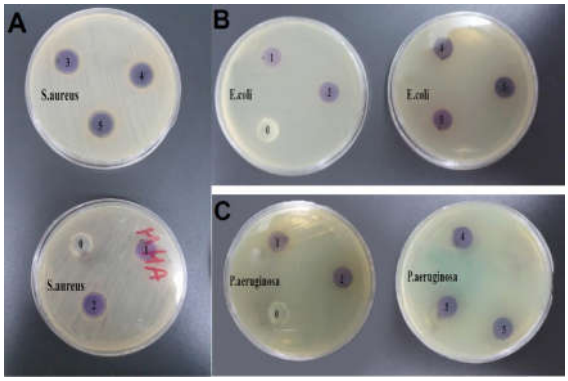

Fig. 9. (A) Antibacterial activity of HAp, CoHAp1, CoHAp2, CoHAp3, CoHAp4 and CoHAp5 by disc diffusion method against S. aureus bacteria (B) Antibacterial activity of HAp, CoHAp1, CoHAp2, CoHAp3, CoHAp4 and CoHAp5 by disc diffusion method against E. coli bacteria

[DOI: 10.22068/ijmse.16.1.39]

4. CONCLUSIONS

Pure and cobalt-doped HAp nanoparticles were synthesized via hydrothermal method. Structure characterization results confirmed the formation of a single phase in the cobalt- doped HAp samples. FESEM images showed rod-like morphology for pure HAP and a change to spherical morphology with the increase in the cobalt content. There was also a particle size reduction with the introduction of Co in the HAp lattice. The substitution of small amounts of Co^{2+} ions into the HAp lattice resulted in powders with paramagnetic properties, as opposed to diamagnetic behaviour in pure HAp samples. According to in-vitro biological assays, no toxicity was induced by Co ions and good adherence of MG63 cells onto the Co- substituted substrates was observed. In addition, nearly twice as much alkaline phosphatase activity was achieved in the presence of Co ions. Finally, the results of antibacterial activity showed an increase in antibacterial activity in Cobalt- doped particles against S. aureus bacteria. However, inefficient antibacterial activity was observed against E. coli and P. aueroginosa is indicated. Based on the results presented, CoHAp may be considered as an attractive apatite based magnetic material to be used in biomedical applications.

5. ACKNOWLEDGEMENT

The authors are grateful to Dr. Mohsen Ahmadi at Shahid Beheshti University of Medical Sciences, Tehran, Iran for his help in conducting antibacterial activity test.

REFERENCES

1. Tang, D., Tare, R. S., Yang, L. Y., Williams, D. F., Ou, K. L. and Oreffo, R. O. C., "Biofabrication of bone tissue: Approaches, challenges and translation for bone regeneration," Biomaterials, 2016, 83, 363–382.
2. Stanovici, J., Le Nail, L. R., Brennan, M. A., Vidal, L., Trichet, V., Rosset, P. and Layrolle, P., "Bone regeneration strategies with bone marrow stromal cells in orthopaedic surgery," Curr Res Transl Med, 2016, 64, 83–90.
3. Li, C. S., Yang, P., Ting, K., Aghaloo, T., Lee, S., Zhang, Y., Khalilinejad, K., Murphy, M. C., Pan, H., Zhang, X., Wu, B., Zhou, Y. H., Zhao, Z., Zheng, Z. and Soo, C., "Fibromodulin reprogrammed cells: A novel cell source for bone regeneration.," Biomaterials,2016, 83, 194–206.
4. Yun, H., Ahn, S., Park, K., Kim, M., Kim, J., Jin, G., Kim, H., Kim, E., "Magnetic nanocomposite scaffolds combined with static magnetic field in the stimulation of osteoblastic differentiation and bone formation.," 2016, 85. Elsevier Ltd, 2016.
5. Zhang, J., Ding, C., Ren, L., Zhou, Y., and Shang, P., "The effects of static magnetic fields on bone," Prog. Biophys. Mol. Biol., 2014, 114, 146–152.
6. Tampieri, A., D'Alessandro, T., Sandri, M., Sprio, S., Landi, E., Bertinetti, L., Panseri, S. and Pe, G., "Intrinsic magnetism and hyperthermia in bioactive Fe-doped hydroxyapatite," Acta Biomater.,2012, 8, 843–851.
7. Russo, A., Bianchi, M., Sartori, M., Parrilli, A., Panseri, S., Ortolani, A., Sandri, M., Boi, M., Salter, D. M. and Maltarello, M. C., "Magnetic forces and magnetized biomaterials provide dynamic flux information during bone regeneration," J. Mater. Sci. Mater. Med., 2016, 27,1–13.
8. Hou, C. H., Hou, S. M., Hsueh, Y. S., Lin, J., Wu, H. C., and Lin, F. H., "The in vivo performance of biomagnetic hydroxyapatite nanoparticles in cancer hyperthermia therapy," Biomaterials, 2009, 30, 23, 3956–3960.
9. Kaygili, O., Dorozhkin, S. V., Ates, T., Al-Ghamdi, A. A., and Yakuphanoglu, F., "Dielectric properties of Fe doped hydroxyapatite prepared by sol-gel method," Ceram. Int., 2014, 40, 9395–9402.
10. Shi, C., Gao, J., Wang, M., Shao, Y., Wang, L., Wang, D. and Zhu, Y., "Functional hydroxyapatite bioceramics with excellent osteoconductivity and stern-interface induced antibacterial ability," Biomater. Sci., 2016, 4, 699–710.
11. Lu, H., Liu, Y., Guo, J., Wu, H., Wang, J., and Wu, G., "Biomaterials with antibacterial and osteoinductive properties to repair infected bone defects," Int. J. Mol. Sci., 2016, 17, 1–18.
12. Geng, Z., Cui, Z., Li, Z., Zhu, S., Liang, Y., Liu, Y., Li, X., He, X., Yu, X., Wang, R. and Yang, X., "Strontium incorporation to optimize the antibacterial and biological characteristics of silver-substituted hydroxyapatite coating," Mater. Sci. Eng. C, 2016, 58, 467–477.
13. Huang, Y., Hao, M., Nian, X., Qiao, H., Zhang, X., Zhang, X., Song, G., Guo, J., Pang, X. and Zhang, H., "Strontium and copper co-substituted hydroxyapatite-based coatings with improved antibacterial activity and cytocompatibility fabricated by electrodeposition," Ceram. Int., 2016, 42, 11876–11888.

[DOI: 10.22068/ijmse.16.1.39]

14. Veselinovic, L., Karanovic, L., Stojanovic, Z., Bracko, I., Markovic, S., Ignjatovic, N., and Uskokovic, D., "Crystal structure of cobalt-substituted calcium hydroxyapatite nanopowders prepared by hydrothermal processing," J. Appl. Crystallogr., 2010, 43, 320–327.
15. Geng, Z., Cui, Z., Li, Z., Zhu, S., Liang, Y., Liu, Y., Li, X., He, X., Yu, X., Wang, R. and Yang, X., "Strontium incorporation to optimize the antibacterial and biological characteristics of silver-substituted hydroxyapatite coating," Mater. Sci. Eng. C, 2016, 58, 467–477.
16. Ignjatović, N., Ajduković, Z., Savić, V., Najman, S., Mihailović, D., Vasiljević, P., Stojanović, Z., Uskoković, V. and Uskoković, D., "Nanoparticles of cobalt-substituted hydroxyapatite in regeneration of mandibular osteoporotic bones," J. Mater. Sci. Mater. Med., 2013, 24, 343–354.
17. Tank, K. P., Chudasama, K. S., Thaker, V. S., and Joshi, M. J., "Cobalt-doped nanohydroxyapatite: synthesis, characterization, antimicrobial and hemolytic studies," J. nanoparticle Res., 2013, 15, 1–11.
18. Stojanović, Z., Veselinović, L., Marković, S., Ignjatović, N., and Uskoković, D., "Hydrothermal Synthesis of Nanosized Pure and Cobalt-Exchanged Hydroxyapatite," Mater. Manuf. Process., 2009, 24, 1096–1103.
19. Kramer, E., Itzkowitz, E., and Wei, M., "Synthesis and characterization of cobalt-substituted hydroxyapatite powders," Ceram. Int., 2014. Vol. 40, Issue 8, 2014, 13471-13480.
20. Kramer, E., Zilm, M., and Wei, M., "A Comparative Study of the Sintering Behavior of Pure and Iron-Substituted Hydroxyapatite," Bioceram. Dev. Appl.,2013, 3, 1–9.
21. Tampieri, A., D'Alessandro, T., Sandri, M., Sprio, S., Landi, E., Bertinetti, L., Panseri, S., Pepponi, G., Goettlicher, J., Bañobre-López, M. and Rivas, J., "Intrinsic magnetism and hyperthermia in bioactive Fe-doped hydroxyapatite," Acta Biomater., 2012, 8,843–851.
22. Sarath Chandra, V., Elayaraja, K., Thanigai Arul, K., Ferraris, S., Spriano, S., Ferraris, M., Asokan, K., S. and Kalkura, N., "Synthesis of magnetic hydroxyapatite by hydrothermal–microwave technique: Dielectric, protein adsorption, blood compatibility and drug release studies," Ceram. Int., 2015, 41, 13153–13163.
23. Petchsang, N., Pon-On, W., Hodak, J. H., and Tang, I. M., "Magnetic properties of Co-ferrite-doped hydroxyapatite nanoparticles having a core/shell structure," J. Magn. Magn. Mater.,2009, 321,1990–1995.
24. Czarnek, K., Terpi Owska, S., and Siwicki, A. K., "Selected aspects of the action of cobalt ions in the human body," Cent. J. Immunol.,2015, 40, 236.
25. Herrmann, W., and Obeid, R.,"Cobalamin Deficiency," in Water Soluble Vitamins SE - 16, vol. 56, O. Stanger, Ed. Springer Netherlands, 2012, pp. 301–322.
26. Chandra, V. S.,"Synthesis of magnetic hydroxyapatite by hydrothermal microwave technique: Dielectric, protein adsorption, blood compatibility and drug release studies," Ceram. Int., 2015, 41, 13153–13163.
27. Ignjatović, N., Ajduković, Z., Savić, V., Najman, S., Mihailović, D., Vasiljević, P., Stojanović, Z., Uskoković, V. and Uskoković, D., "Nanoparticles of cobalt-substituted hydroxyapatite in regeneration of mandibular osteoporotic bones," J. Mater. Sci. Mater. Med., 2013, 24, 343–354.
28. Kulanthaivel, S., Mishra, U., Agarwal, T., Giri, S., Pal, K., Pramanik, K. and Banerjee, I., "Improving the osteogenic and angiogenic properties of synthetic hydroxyapatite by dual doping of bivalent cobalt and magnesium ion," Ceram. Int., 2015. Vol. 41, Issue 9, 11323-11333.
29. Montazeri, L., Javadpour, J., Shokrgozar, M. Bonakdar, A., S., and Javadian, S., "Hydrothermal synthesis and characterization of hydroxyapatite and fluorhydroxyapatite nano-size powders.," Biomed. Mater.,2010, 5, 45004.
30. Wallin, R. F., and Arscott, E. F., "A practical guide to ISO 10993-5: cytotoxicity," 1998, 20, 96-97.
31. Stojanovi, Z., Veselinovi, L., Markovi, S., Ignjatovi, N., and Uskokovi, D., "Hydrothermal synthesis of nanosized pure and cobalt-exchanged hydroxyapatite," Mater. Manuf. Process., 2009, 24, 1096–1103.
32. Akkouch, A., Zhang, Z., and Rouabhia, M., "Engineering bone tissue using human dental pulp stem cells and an osteogenic collagen-hydroxyapatite-poly (L-lactide-co-ε-caprolactone) scaffold.," J. Biomater. Appl.,2014, 28, 922–36.
33. Sadeghi, D., Nazarian, H., Marouf, N., Aghalu, F., and Nojehdehyan, H., "AlkalinePhosphatase Activity of Osteoblast Cells on Three-Dimensional Chitosan-Gelatin / Hydroxyapatite Composite Scaffolds Introduction :," J. Dent. Sch., 2013, 30, 203–209.
34. Filová, E., Suchý, T., Sucharda, Z., Šupová, M., Žaloudková, M., Balík, K., Lisá, V., Šlouf, M. and Bačáková, L., "Support for the initial attachment, growth and differentiation of MG-63 cells: A

[DOI: 10.22068/ijmse.16.1.39]

comparison between nano-size hydroxyapatite and micro-size hydroxyapatite in composites," Int. J. Nanomedicine, 2014,9, 3687–3706.
35. Nikkhah, M., Edalat, F., Manoucheri, S., and Khademhosseini, A., "Engineering microscale topographies to control the cell substrate interface," Biomaterials, 2012, 33, 5230–5246.
36. Kolmas, J., Groszyk, E., and Kwiatkowska-R ycka, D., "Substituted Hydroxyapatites with Antibacterial Properties," Biomed Res. Int., 2014, 1-15.
37. Stanić, V., Dimitrijević, S., Antić-Stanković, J., Mitrić, M., Jokić, B., Plećaš, I. B. and Raičević, S., "Synthesis, characterization and antimicrobial activity of copper and zinc-doped hydroxyapatite nanopowders," Appl. Surf. Sci., 2010, 256, 6083–6089.

[DOI: 10.22068/ijmse.16.1.39]